Nonlinear resonant Auger spectroscopy in CO using an x-ray pump-control scheme

3 authors:

Song Bin Zhang
Shaanxi Normal University
26 PUBLICATIONS   **195** CITATIONS

Victor Kimberg
KTH Royal Institute of Technology
67 PUBLICATIONS   **456** CITATIONS

Nina Rohringer
Max Planck Institute for the Physics of Compl…
63 PUBLICATIONS   **1,981** CITATIONS

Some of the authors of this publication are also working on these related projects:

Project   X-ray Spectrosopy View project

Project   Nonlinear Optics View project

Nonlinear resonant Auger spectroscopy in CO using an x-ray pump-control scheme

Song Bin Zhang,[1,2,3,*] Victor Kimberg,[4,5] and Nina Rohringer[2,3,†]

[1]*School of Physics and Information Technology, Shaanxi Normal University, 710119 Xi'an, China*
[2]*Max Planck Institute for the Structure and Dynamics of Matter (MPSD), 22761 Hamburg, Germany*
[3]*Center for Free-Electron Laser Science (CFEL), 22761 Hamburg, Germany*
[4]*Department of Theoretical Chemistry and Biology, School of Biotechnology, Royal Institute of Technology, S-106 91 Stockholm, Sweden*
[5]*Laboratory for Nonlinear Optics and Spectroscopy, Siberian Federal University, Krasnoyarsk 660041, Russia*

In the present paper we propose nonlinear femtosecond x-ray pump-probe spectroscopy to study the vibrational dynamics of a core-excited molecular state and discuss numerical results in CO. A femtosecond pump resonantly excites the carbon core-excited $1s$-$1\pi^*$ state of the CO molecule. A second strong probe (control) pulse is applied at variable delay and is resonantly coupled to a valence excited state of the molecule. The strong nonlinear coupling of the control pulse induces Rabi flopping between the two electronic states. During this process, a vibrational wave packet in the core-excited state is created, which can be effectively manipulated by changing the time delay between pump and control pulses. We present an analysis of the resonant Auger electron spectrum and the transient absorption or emission spectrum on the pump transition and discuss their information content for reconstruction of the vibrational wave packet.

I. INTRODUCTION

Since their advent, x-ray free-electron lasers (FELs) have developed into quite versatile x-ray sources that deliver wavelength-tuneable x-ray pulses of durations ranging from a few to several hundred femtoseconds (fs) [1–3]. Recently, schemes have also been invented allowing for the creation of two x-ray pulses of tuneable frequency and time delay for 50- to 100-fs-long pulses [4] and a few-femtosecond pulses [5]. Moreover, self-seeding in the hard- [6] and soft-x-ray range [7] gives pulses of improved temporal coherence, and several schemes have been proposed to produce transform-limited attosecond and femtosecond pulses [8–10]. These versatile x-ray sources will therefore soon open the pathway for implementing all x-ray pump-probe schemes. One very successful scheme turns out to be splitting of the FEL pulse into two replicas and using them as time-delayed pump and probe pulses; this scheme has been successfully applied to study interatomic Coulombic decay in neon dimers [11], charge transfer in iodine molecules [12] and iodomethane [13], photoexcited molecular dynamics [14] and so on; an even more elaborated scheme, which makes use of a pair of x-ray pulses with slightly different wavelengths [15–19], was used to probe ultrafast electronic and molecular dynamics [19–23]. Here, we propose a different x-ray pump-probe scheme based on two time-delayed x-ray pulses of different frequencies [15–18] to study vibrational wave-packet dynamics in core-excited electronic states. In this scheme (see Fig. 1) a fs pump pulse resonantly excites a core-excited state R. A time-delayed probe (control) pulse of variable intensity then couples the core-excited state R to a valence excited electronic state F, thereby coherently transferring population from the ground state to the valence excited state F. In contrast to conventional pump-probe schemes, the intensity of the probe pulse is strong to allow for

nonlinear coupling and Rabi flopping between the core-excited state R and the valence excited state F, resulting in the creation of vibrational wave packets in both states. Due to this, we call the probe pulse the control pulse in what follows. Note that the Auger spectra can be changed with only one strong pump pulse (maybe with a further weak probe pulse), Rabi splitting appears in the spectra as studied in the atomic and molecular cases [24–27]; however, with the present weak-pump strong-control scheme, as the study shows, we can get the degree to control the Auger spectra. The core-excited state R has a short lifetime and predominantly decays via Auger decay, resulting in the so-called resonant Auger scattering (RAS) process. RAS spectroscopy is successfully applied to study the nuclear wave-packet dynamics in core-excited states [28] as well as in final ionic valence excited states [29]. Here we study the resonant Auger electron spectrum and the spectrum of the transmitted pump pulse (transient absorption or emission spectroscopy) that both encode information of the core-excited vibrational wave packet. Specifically, we study this pump-probe scheme in the CO molecule, where the weak pump pulse is tuned at $\omega_1 = 287.4$ eV to excite the ground electronic state I ($X^1\Sigma^+$) to the carbon core-excited state R (C $1s^{-1}\pi^{*1}\Pi$), and the control pulse tuned at around $\omega_2 = 277.6$ eV couples state R to the valence excited state F ($1\pi^{-1}\pi^*\,I^1\Sigma^-$). The core-excited state R predominantly decays via an Auger process to the ground ionic state A ($1\pi^{-1}\,^2\Pi$) with a lifetime of about 8.2 fs [30].

The role of the weak pump pulse is only to create the initial wave packet in the core-excited state, while the manipulation of the wave-packet dynamics is performed with the help of the strong control pulse. The wave packet in the core-excited state can be manipulated by the pulse area of the control pulse (time-integrated intensity profile): if the control pulse is chosen as a π pulse, it can only transfer the electronic population from the core-excited state R down to the final state F, and the dynamics of the core-excited state will not be changed. However, when the control-pulse intensity is chosen so that it allows for a full Rabi cycle transferring the population back to the core-excited state (e.g., a 2π pulse), the dynamics of the

*song-bin.zhang@snnu.edu.cn
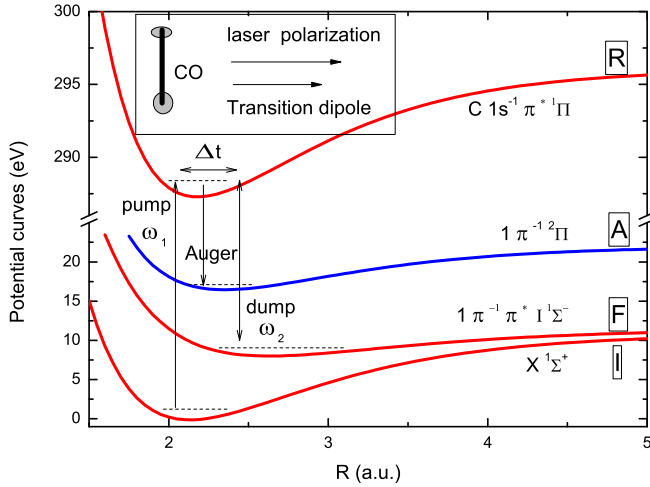†nina.rohringer@mpsd.mpg.de

FIG. 1. Potential-energy curves for the four involved electronic states and the schematics of the present pump-probe scheme. The optical nonlinear interaction is caused by the strong probe (control) pulse on the transition between states R and F. The wave-packet dynamics in state R can be monitored either by the RAS spectrum to the state A or the transient absorption signal of the pump radiation. All potential curves are described by the Morse potentials with the parameters taken from Ref. [38].

core-excited wave packet can be altered by the control pulse. In the following we show that the nonlinearity caused by the strong control pulse on the transition between the core-excited state R and the valance excited state F can effectively change the wave-packet dynamics of the core-excited state, which is reflected in the RAS spectra.

In addition to the RAS spectrum, we study the transient absorption or emission spectrum of the transmitted radiation. Since the technique of transient absorption with strong infrared (IR) pump and weak extreme ultraviolet (XUV) probe has been successfully applied to study the Fano lineshape [31] and control the time-dependent two-electron wave packet [32], we can expect the technique of all-x-ray transient absorption to play important roles in the near future. In principle, both the transmitted pump pulse and control pulse encode information of the core-excited wave-packet dynamics. The control pulse, however, encodes vibrational wave-packet dynamics of both the core and valence excited states, so that it is more difficult to unravel the wave-packet dynamics in both states. We therefore study the absorption or emission spectrum of the weak pump pulse, which only reflects wave-packet dynamics in the core-excited state. The absorption or emission spectrum is numerically studied by calculating the molecular dipole response function [33–35]. In this first study, we omit propagation effects, which could appear by propagation through an optically dense medium [36,37]. Despite this simplification, it turns out that the RAS is much easier to interpret than the transient absorption or emission spectrum.

The numerical method is briefly introduced in the next section, followed by a discussion of the numerical results and a conclusion. Unless otherwise stated, atomic units (a.u.) are used throughout the paper.

II. THEORETICAL METHOD

The time-dependent wave-packet-propagation method [25,26,39] is employed to evaluate the dynamics of the electronic states and the RAS spectrum. Within the Born–Oppenheimer approximation, the total wave function $\Psi(t)$, including the four electronic states (the ground, resonant, and final valance excited sates with the stationary electronic wave functions Φ_I, Φ_R, and Φ_F, respectively, and the ionic state produced by the emission of Auger electrons of energy ε and electronic wave function Φ_A^ε) can be expanded as

$$\Psi(t) = \Psi_I(t)\Phi_I + \Psi_R(t)e^{-i\omega_1 t}\Phi_R + \Psi_F(t)e^{-i(\omega_1-\omega_2)t}\Phi_F$$
$$+ \int \Psi_A(\varepsilon,t)e^{-i\omega_1 t}\Phi_A^\varepsilon d\varepsilon. \tag{1}$$

Here, $\Psi_I(t)$, $\Psi_R(t)$, $\Psi_F(t)$, and $\Psi_A(\varepsilon,t)$ are the time-dependent nuclear wave packets propagating on the respective electronic surfaces. The time-dependent norm of $\Psi_X(t)$ corresponds to the time-dependent occupation probabilities of the electronic state $X = (I,R,F,A)$. In the ansatz of the total wave function we separated a rapid-evolving phase factor $e^{-i\omega_1 t}$ or $e^{-i(\omega_1-\omega_2)t}$ [25,26,40–43].

We suppose a linearly polarized electric field $G_i(t) = g_{0i}g_i(t)\cos(\omega_i t)$ ($i = 1$ and 2, representing the index for the pump and control pulses, respectively) with pulse envelope $g_i(t)$ and electric-field strength g_{0i}. Inserting the total wave function into the time-dependent Schrödinger equation for the total Hamiltonian and implying the rotating-wave approximation [44,45] and the local approximation [39,40,46,47] leads to the following set of equations determining the evolution of the wave packets:

$$\dot{\Psi}_I(t) = \left[\widehat{\mathbf{T}}(R,\theta) + V_I(R) - \frac{i}{2}\Gamma_{\text{ph}}(t)\right]\Psi_I(t)$$
$$+ D_{1x}^\dagger(t)\sin\theta\,\Psi_R(t),$$
$$\dot{\Psi}_R(t) = D_{1x}(t)\sin\theta\,\Psi_I(t)$$
$$+ \left[\widehat{\mathbf{T}}(R,\theta) + V_R(R) - \frac{i}{2}\Gamma_{\text{Aug}} - \omega_1\right]\Psi_R(t)$$
$$+ D_{2x}^\dagger(t)\sin\theta\,\Psi_F(t),$$
$$\dot{\Psi}_F(t) = D_{2x}(t)\sin\theta\,\Psi_R(t)$$
$$+ [\widehat{\mathbf{T}}(R,\theta) + V_F(R) - (\omega_1-\omega_2)]\Psi_F(t),$$
$$\dot{\Psi}_A(\varepsilon,t) = V\Psi_R(t) + [\widehat{\mathbf{T}}(R,\theta) + V_A(R) + \varepsilon - \omega_1]\Psi_A(\varepsilon,t).$$

Here R is the nuclear distance, θ is the angle between the molecular axis and the polarization of the pulse, $\widehat{\mathbf{T}}(R,\theta)$ is the nuclear kinetic operator for the vibrational and rotational motions, $V_I(R)$, $V_R(R)$, $V_F(R)$, and $V_A(R)$ are the potential-energy curves (PECs) of the electronic states (see Fig. 1), the functions $D_{ix}(t) = d_i g_{0i} g_i(t)/2$ ($i = 1,2$), with the the dipole transition elements $d_1 = \langle\Phi_R|\hat{x}|\Phi_I\rangle$ and $d_2 = \langle\Phi_F|\hat{x}|\Phi_R\rangle$, $V = \langle\Psi_A^\varepsilon|1/\hat{r}_{12}|\Phi_R\rangle$ is the Coulomb matrix element between the core-excited state and the final ionic state, $\Gamma_{\text{Aug}} = 2\pi|V|^2$ is the Auger decay width, which is 0.08 eV in the case considered, corresponding to an Auger lifetime of about 8.2 fs, and $-\frac{i}{2}\Gamma_{\text{ph}}(t)$ represents the time-dependent leakage due to direct photoionization [25,26]. Since the wave-packet dynamics in the present study evolve around the equilibrium

region of the CO molecule, it would be a good approximation to neglect the nuclear coordinate dependence of those parameters, explicitly, $d_1 = 0.1$ a.u., $d_2 = 0.03$ a.u., and $V = 0.007$ a.u. [25].

Finally the RAS spectrum can be computed as the norm of the wave packet $\Psi_A(\varepsilon,t)$ at long times [25,26,39]:

$$\sigma_A(\varepsilon) = \lim_{t\to\infty} \langle \Psi_A(\varepsilon,t) | \Psi_A(\varepsilon,t) \rangle. \tag{2}$$

The total Auger electron yield is given by

$$\sigma_A^T = \int \sigma_A(\varepsilon) d\varepsilon. \tag{3}$$

The system of Eq. (2) is solved numerically employing Gaussian pulses $g_1(t) = g_2(t) = e^{-t^2/\tau^2}$ of $\tau = 1.7$ fs (the full width at half-maximum of the pulse is ~ 2.83 fs) by multiconfiguration time-dependent Hartree (MCTDH) [48]. The pulse durations and the delay times between the pulses are much shorter than any involved rotational periods of the molecule, so that the molecular alignment or orientation with respect to the laser polarization can be regarded as constant during the interaction with the two pulses. Note that impulsive laser alignment techniques allow us to achieve quite high field-free laser alignment [49]. We suppose that the ensemble of molecules is aligned perpendicularly to the laser polarization axis (or $\theta = \pi/2$). Initially, the molecule is in its ground electronic and vibrational states.

III. NUMERICAL RESULTS

The field intensity (defined in terms of the Rabi frequency $\Omega_i = d_i g_{0i}$, $i = 1,2$) of the weak resonant ultrashort pump pulse is fixed and chosen to be $\Omega_1 = 0.005$ a.u. or 0.136 eV (corresponding to a Rabi period of ~ 30.0 fs), so that the depletion of the ground state is within 10%. Our calculations show that this pulse directly ionizes the ground state by less than 0.01%, thus depletion of the ground state is dominantly induced by the core excitation, followed by the Auger decay of the core-excited state. As discussed in the previous part, the ability of transferring the electrons back to the core-excited state R through the intermediate valance excited state F is controlled by changing the intensity of the control pulse. The special cases of a π pulse and a 2π pulse are the simplest cases. For our numerical study we choose pulses with Rabi frequencies of $\Omega_2 = 0.025$ and 0.05 a.u., with Rabi periods of about 6.0 and 3.0 fs, respectively. Figure 2 shows the total Auger electron yields as a function of the control-pulse frequency ω_2 and the time delay Δt for these two different control intensities. As can be seen in Fig. 2, the total Auger yields experience a minimum at around $\omega_2 = 277.6$ eV and $\Delta t = 1.0$ fs which is selected as the optimized frequency for the control pulse in the remainder of this work, while the delay time is varied. The weak and strong control pulses induce different dynamics between states R and F, different populations are transferred from state R to state F, resulting in the big changes of the total Auger yields between the two cases with different control pulses.

The RAS spectra modified by the ultrashort control pulse are shown in Figs. 3 and 4 for different time delays with control intensities $\Omega_2 = 0.025$ and 0.05 a.u., respectively. When the control pulse arrives before the pump pulse (for $\Delta t = -2.0$ fs),
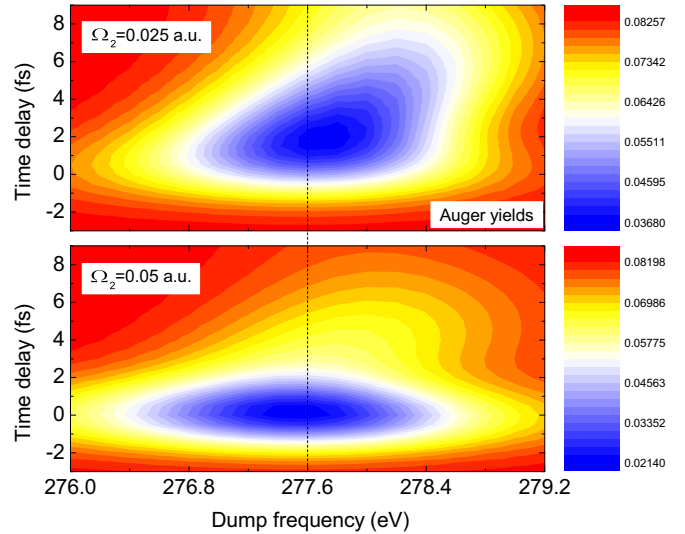

FIG. 2. The total Auger yields as a function of the photon energy ω_2 of the control pulse and the time delay between the two x-ray pulses for the two values of the control field intensities. The minimum of the Auger yield, and highest transfer of electrons from state R to state F, is around $\omega_2 = 277.6$ eV. Calculations show that the depletion of the ground state by direct ionization is less than 0.01%.

the population of the R state is negligible and the control pulse does not interact resonantly with the molecule. In this case, the RAS spectra for the both control intensities show very similar structure, corresponding to the conventional measurements [50] in the weak-field regime with synchrotron radiation. The only exception is an additional peak around 271.1 eV in the present calculations, which appears due to the resonant weak vibrational excitation of the $\nu = 1$ vibrational level in the core-excited state by the broad ultrashort control pulse.
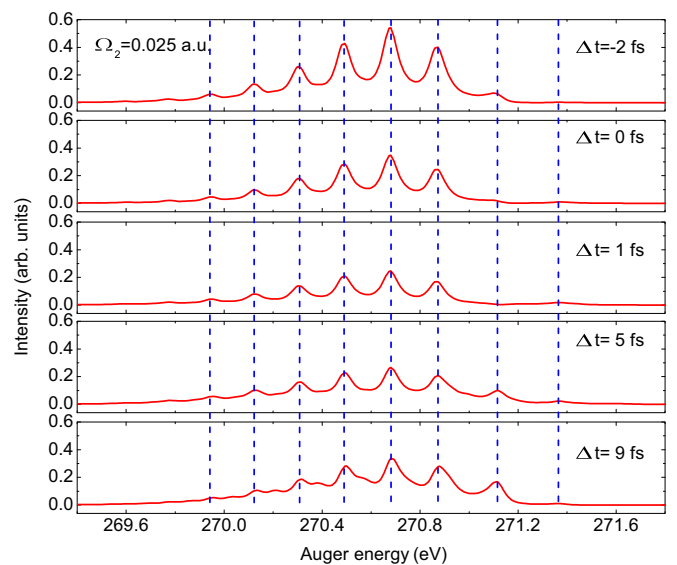

FIG. 3. The resonant Auger spectra for different time delays Δt for a weak control pulse of $\omega_2 = 277.6$ eV and $\Omega_2 = 0.025$ a.u. The vibrationally resolved peaks for the conventional RAS are labeled as the vertical dash lines.
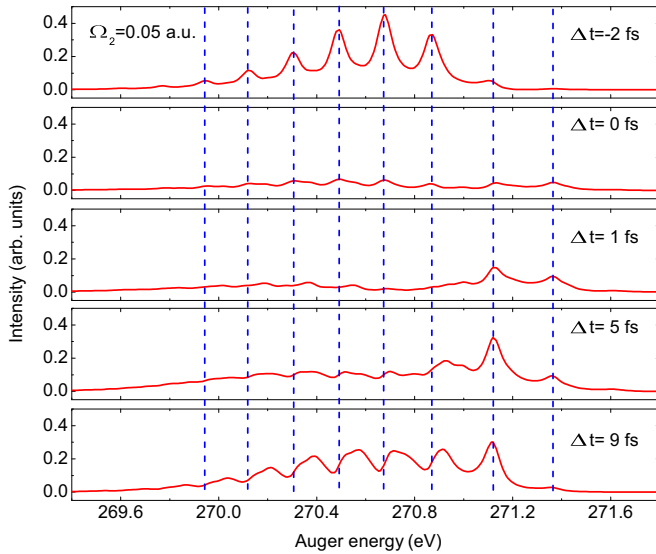
FIG. 4. Same as in Fig. 3, but for a strong control pulse of $\Omega_2 = 0.05$ a.u.

As expected, in the case with the weak control intensity (or $\Omega_2 = 0.025$ a.u.; see Fig. 3), the structures of the Auger spectra do not change much for different Δt, but for an overall drop in spectral intensity with increasing Δt. It is consistent with the decreases of the total Auger yields by varying Δt shown in Fig. 2 for $\omega_2 = 277.6$ eV.

In the case with the strong control intensity ($\Omega_2 = 0.05$ a.u.; see Fig. 4), the shape of the Auger spectra change significantly for different Δt. When the two pulses are fully overlapped (or $\Delta t = 0.0$ fs), a totally new spectrum appears, no main structures exist, the intensities for all the peaks are comparable, and one additional peak shows up at around 271.35 eV. When Δt is increased to 1.0 fs, the spectrum changes again, the intensity of the peak at around 271.1 eV increases considerably, and the peaks below 271.1 eV entirely shift up in energy by about 0.05 eV. Such changes are even more significant when Δt is further increased to 5.0 and 9.0 fs. All these changes are directly related to the effect of the ultrashort control pulse, which repopulates the different vibrational states of the core-excited state when transferring the electrons back to the intermediate state R, and thereby changing its vibrational wave packet, which is reflected in the RAS spectrum.

The vibrationally resolved structures of the Auger spectrum can be understood from the Franck-Condon factors between the core-excited state R and the final RAS ionic state A [50]. Supposing $|v\rangle_X$ refers to the vibrational state $|v\rangle$ of electronic state X, $|_X\langle v'|v\rangle_Y|^2$ denotes the Franck-Condon factors (FCFs) between electronic states Y and X. Figure 5 shows the FCFs $|_R\langle v'|v=0\rangle_I|^2$ and $|_A\langle v'|v\rangle_R|^2$, calculated with the potential energy curves shown in Fig. 1. Since the FCF $|_R\langle v'=0|v=0\rangle_I|^2$ dominates all the other FCFs $|_R\langle v'|v=0\rangle_I|^2$, the weak pump pulse transfers the electrons from the state $|v'=0\rangle_I$ mainly to the state $|v=0\rangle_R$, same as in conventional x-ray absorption spectroscopy (XAS), where the absorption of a monochromatic pulse is studied as a function of incoming photon energy, the conventional RAS spectrum [50] shows a strong

similarity to the distribution of the FCFs $|_A\langle v'|v=0\rangle_R|^2$ (see black bars of the middle panel and cycle line in the lower panel of Fig. 5). However, if more than one vibrational state of the electronic state R is populated, one can expect drastic change of the RAS spectra due to contribution from the higher excited vibrational states $|v\rangle_R$ (see red, blue, and green bars in Fig. 5).

Returning to the present work, the weak pump pulse prepares the initial vibrational states in state R mainly in $v = 0$, the control pulse time delayed by Δt repopulates those vibrational states in state R. The vibrational occupation probabilities of state R and the Franck-Condon factors $|_A\langle v'|v\rangle_R|^2$ can help us to qualitatively understand the changed RAS spectra. The vibrational occupation probabilities of state R after the different time-delayed control pulses are shown in Figs. 6 and 7 for the cases with weak and strong control intensities, respectively.

As revealed in Fig. 6, the weak control pulse does not change the dominant nature of state $|v=0\rangle_R$. The occupation probability of state $|v=1\rangle_R$ is not negligible. This is consistent with the findings in Fig. 3 that the structures of the RAS spectra for different Δt are similar and close to the spectrum measured in the weak field. The additional peak in the spectra at around 271.1 eV can be assigned to the initial occupation of the $v = 1$ state by the broadband pump pulse, and its intensity is dominated by FCFs $|_A\langle v'=0|v=1\rangle_R|^2$. When $\Delta t = 9.0$ fs, the occupation probability of state $|v=0\rangle_R$ is still larger than that of $|v=1\rangle_R$, but comparable in size, which results in the small structures at around 270.2, 270.4, and 270.6 eV in the spectrum shown in Fig. 3 for $\Delta t = 9.0$ fs. And when Δt is big or the control pulse is far behind the pump pulse, coherent evolution of the field-free system plays the major role, some population from the $|v=0\rangle_R$ state goes into the $|v=1\rangle_R$ state and the population of $|v=1\rangle_R$ is increasing over time.

The strong control pulse largely changes the occupation probabilities of states $|v\rangle_R$, as shown in Fig. 7. In the case of time delay $\Delta t = 0.0$ fs, the occupation probability of state $|v=0\rangle_R$ decreases a lot with respect to the pump-only spectrum and is only a little larger than that of states $|v=1,2\rangle_R$. When $\Delta t = 1.0$ fs, the occupation probability of state $|v=0\rangle_R$ even becomes negligible at times long after the control pulse has passed. When $\Delta t \geqslant 1.0$ fs, state $|v=1\rangle_R$ becomes the dominant one after the control pulse has passed, the peak in the spectra shown in Fig. 4 at around 271.1 eV becomes more pronounced. The control pulse also repopulates state $|v=2\rangle_R$ considerably when $\Delta t = 1.0$ and 5.0 fs, which explains the significance of the peak in the spectra shown in Fig. 4 at around 271.35 eV contributed by the transition $|v=2\rangle_R \rightarrow |v'=0\rangle_A$ when $\Delta t = 0.0, 1.0$, and 5.0 fs. For control pulses with delays $\Delta t \geqslant 1.0$ fs, several states $|v\rangle_R$ become important. Their corresponding FCFs are different both in positions and intensities. This results in the shifting of the peaks in the spectra shown in Fig. 4 below 271.1 eV from the coherent contributions of those higher vibrational states.

Let us turn to x-ray transient absorption spectra (XTAS) to trace the nuclear dynamics studied above, similarly as done in conventional transient absorption spectroscopy [34,35]. In particular, we consider here the XTAS as a tool to monitor the core-excited wave packet. The single-molecule photon transient absorption or emission spectrum $S(\omega)$ can be
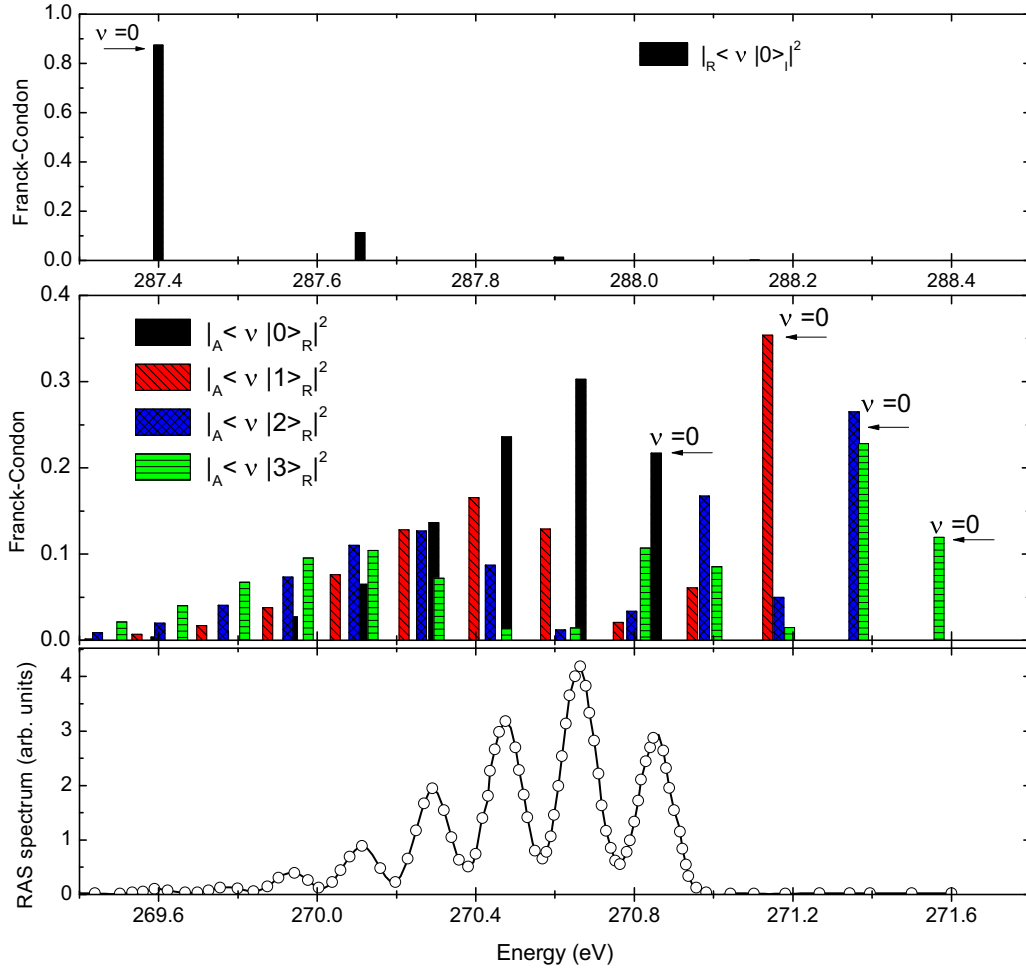
FIG. 5. The Franck-Condon factors $|_R\langle\nu'|\nu=0\rangle_I|^2$ between the initial state I and the core-excited state R (upper panel) and $|_A\langle\nu'|\nu\rangle_R|^2$ between the core-excited state R and final ionic state A (middle panel). The conventional RAS spectrum [50] is also illustrated (lower panel).

expressed as [33–35]

$$S(\omega) = -2\text{Im}[\mu(\omega)E^*(\omega)], \qquad (4)$$

where $\mu(\omega)$ and $E(\omega)$ are the Fourier transforms of the time-dependent induced dipole $\mu(t) = \langle\Psi(t)|\hat{\mu}|\Psi(t)\rangle$ and

the electric field $E(t)$, respectively. Considering the studies in this work, the induced dipole can be simplified as $\mu(t) = \mu_{\text{IR}}(t) + \mu_{\text{RF}}(t) = 2d_1\text{Re}[\langle\Psi_I(t)|\Psi_R(t)\rangle e^{i\omega_1 t}] + 2d_2\text{Re}[\langle\Psi_R(t)|\Psi_F(t)\rangle e^{i\omega_2 t}]$, where the first and second terms correspond to the induced dipoles from the transitions between states I and R and states R and F, respectively.
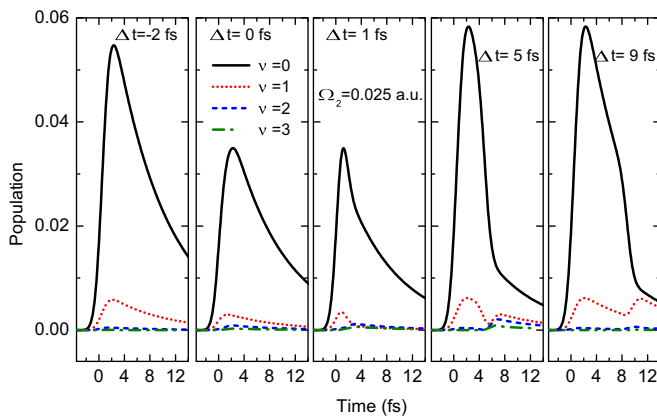

FIG. 6. The vibrational occupation probabilities of the core-excited state R for weak control pulse of photon energy $\omega_2 = 277.6$ eV and an intensity corresponding to $\Omega_2 = 0.025$ a.u.
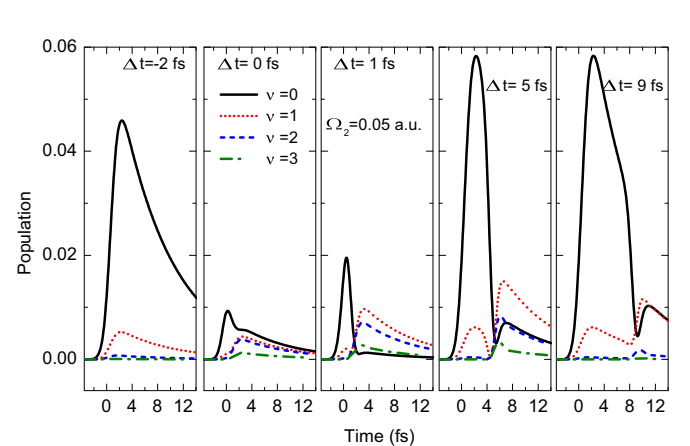

FIG. 7. Same as in Fig. 6, but for strong control pulse $\Omega_2 = 0.05$ a.u.
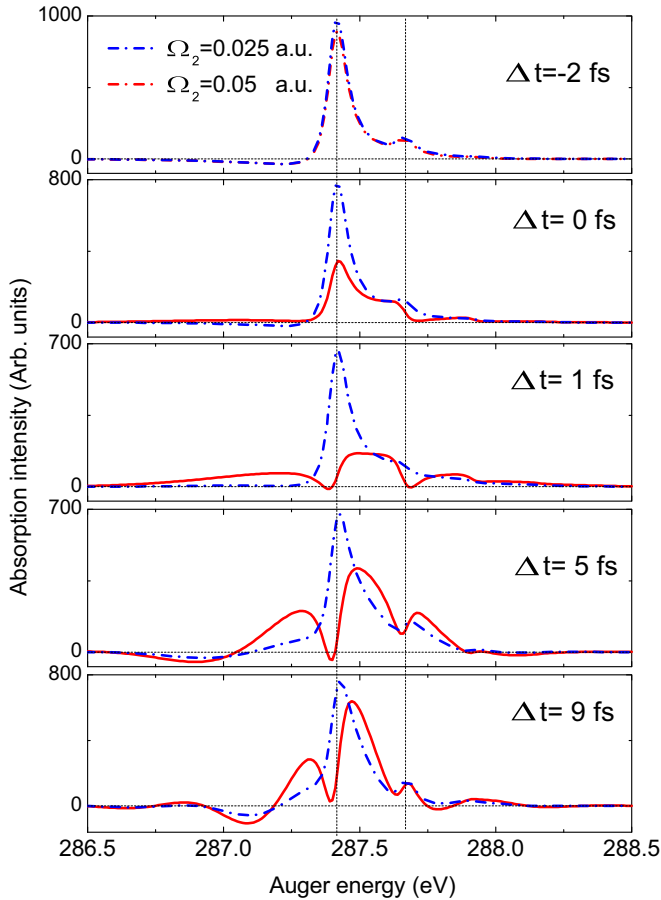
FIG. 8. X-ray transient absorption or emission spectra of CO for the pump field around 287.4 eV. Shown is a comparison for weak and strong control pulses. The absorption or emission peaks for the case of $\Delta t = -2$ fs are labeled as vertical dashed lines.

The spectral components of the pump and control transition are energetically well separated, i.e., $\mu_{IR}(\omega)$ at around 287.4 eV and $\mu_{RF}(\omega)$ at around 277.6 eV. The depletion of the electronic ground state by the pump is weak, so that there are basically no higher-lying vibrational states excited in the electronic ground state. The control pulse, on the contrary, can induce Rabi flopping between states R and F, which results in a change of the vibrational wave packets of both states R and F. Since both transition dipoles μ_{IR} and μ_{RF} monitor the core-excited state, they can be analyzed to learn about the nonlinear response induced by the control pulse. Since there is no vibrational wave packet in the ground state, study of the absorption spectrum given by $\mu_{IR}(\omega)$ at around 287.4 eV is the simplest choice, to monitor the vibrational wave packet in state R. Analyzing the dipole $\mu_{RF}(\omega)$ at around 277.6 eV gives information of vibrational wave packet induces in states R and F and is quite difficult to interpret.

Figure 8 shows the XTAS of the pump field around 287.4 eV for both the weak and strong control pulses and for different time delays. As clearly shown in the plots, the absorption spectra for the weak control pulses ($\Omega_2 = 0.025$ a.u.) show two peaks, which correspond to the vibrational transitions $|v' = 0\rangle_I \rightarrow |v = 0\rangle_R$ and $|v' = 0\rangle_I \rightarrow |v = 1\rangle_R$, and the relative intensities are determined by the Frank–Condon

factors $|_I\langle v' = 0|v = 0, 1\rangle_R|^2$. The absorption profile obtained by using Eq. (4) coincides with conventional $C1s \rightarrow \pi^*$ absorption spectroscopy [51]. The negative parts in the spectra around 287.2 eV mainly come from the emissions $|v = 1\rangle_R \rightarrow |v' = 1\rangle_I$. The changes of the absorption spectra for strong control pulses ($\Omega_2 = 0.05$ a.u.) are quite complex. Increasing Δt, the two main peaks shift and split into multiple peaks, the spectra become dominated by the nonlinear Autler–Townes splitting, the vibrational transitions cannot be identified from the absorption peaks anymore, and it is not straightforward to determine the changes of the vibrational occupation probabilities by a simple analysis. In contrast, at the same condition, the resonant Auger spectroscopy (shown in Fig. 7) still clearly shows the vibrational structure, and the position and occupation of the vibrational states in the core-excited electronic state can be inferred from the spectrum. RAS spectroscopy is therefore a powerful complementary technique to transient absorption spectroscopy and can, as demonstrated in this case, have a simpler interpretation as compared with the transient absorption spectrum.

Before making conclusions, we should note that, although the XTAS for a strong control pulse ($\Omega_2 = 0.05$ a.u.) is complex from the aspect of Autler–Townes splitting, it manifests clearly an asymmetric lineshape with the changes of Δt, similar to the Fano profile resulting from the interference of the transition to the bound state embedded in the continuum [32,34,52–54]. As was recently approved, the laser control allows us to manipulate the interference and as the results of changing the lineshape of the transient absorption spectra from the Lorentz to Fano profile [31,55,56]. In the present case of CO, the final bound state F, with a large shift of the PEC equilibrium from the ground state and core-excited state and a shallow PEC with the vibrational frequency much smaller than the bandwidth of the control pulse, can be considered as a quasicontinuum, similar to the molecular dissociative continuum, where the Fano profile for the populations dynamics was observed earlier [57]. Due to the presence of the strong laser field, the discrete state R is embedded in a quasicontinuum state F [also called a light-induced continuum structure (LICS) [58,59]], resulting in the observed Fano profile of the XTAS.

A simplified model and simulation depicted in Fig. 9 is performed to illustrate the above statements. Here we use the one-level approximation for the ground state I and resonant core-excited state R, while vibrational manifold of the final state F is fully taken into account. The same pulse parameters for the pump and control pulses of Fig. 8 are employed here. The case of a single discrete level embedded in a spectral continuum in this case can be described by the well-known Fano formula [52,53], derived for the case of an autoionization state:

$$\sigma(\varepsilon) = \sigma_0 \frac{(q + \varepsilon)^2}{1 + \varepsilon^2}, \quad (5)$$

where $\varepsilon = 2(\omega - \omega_{IR})/\Gamma_{Aug}$ describes the detuning of the pump field from the 0-0 vibrational transition between I and R states [Fig. 9(a)]. Figure 9(b) shows the simulated XTAS from the simplified model and the fitting to the Fano profile of Eq. (5), using the complex values of the Fano parameter q stated in the figure caption. Very good agreements are achieved. Note that, contrary to field-free case, the laser field
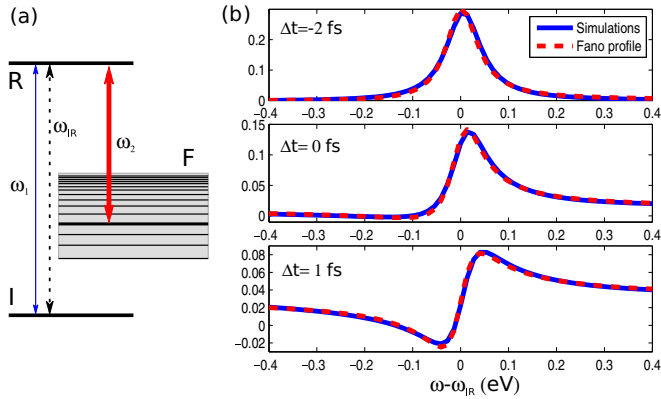
FIG. 9. Fano profiles in XTAS. (a) Simplified two-level plus quasicontinuum model of the Fano interference profile in XTAS of CO. (b) Simulated XTAS for model (a) with the same pulse parameters as for Fig. 8 compared against the fitted Fano profile of Eq. (5) as a function of the detuning of the probe field $\Delta\omega = \omega - \omega_{IR}$. The following values of the Fano parameter q are used: $\Delta t = -2$ fs, $q \to \infty$; $\Delta t = 0$ fs, $q = 3.8 + 1.8i$; $\Delta t = 1$ fs, $q = 1.7 + 1.5i$. The control field intensity $\Omega_2 = 0.05$ a.u.

induces additional phase between the discrete and continuum states, resulting in a complex Fano parameter q [57,59,60] depending on the pulse intensity and also the time delay Δt between the pulses. Back to the real system, the XTAS (Fig. 8) is much more complex as compared with the simplified model simulations (Fig. 9), which can be simply understood from the fact that, in reality, several vibrational levels in the core-excited state are populated (Fig. 7) bringing up much more complex interference phenomena. Further theoretical investigations of XTAS are necessary to fully understand this technique on the studies of molecules.

IV. CONCLUSIONS

In the present paper we propose a nonlinear x-ray pump-probe scheme based on resonant Auger electron spectroscopy and discussing numerical results for the CO molecule. A relatively weak pump pulse resonantly excites a CO molecule to a core-excited state. A second time-delayed control pulse resonantly couples this core-excited state to a valence excited state, allowing for the Rabi flopping between both states. During this process of coherent population transfer, vibrational

wave packets in the core-excited and valence excited states are induced. Both the resonant Auger spectrum and the transient absorption or emission spectrum of the pump pulse give valuable information on the core-excited vibrational wave-packet dynamics. We present a detailed numerical study of this pump-probe scheme, and the RAS and absorption or emission spectra were interpreted in terms of vibrational Frank–Condon overlaps. Both spectra show a strong sensitivity to the delay time between pulses. In the case of a weak control pulse (with a pulse area corresponding to less than that of a π pulse), the Auger spectrum is hardly affected, only showing a drop in the spectral intensity according to the loss of the core-excited state population due to the resonant transfer to the lower-lying state. For stronger intensities of the control pulse, the vibrational distribution of the upper state is shuffled by revolving the population via the resonantly coupled vibrationally excited state. This results in a coherent change of the wave packet in the core-excited state, with clear interference effects in the according RAS spectra. Compared to transient absorption or emission spectroscopy of the weak pump pulses, the RAS spectra provide a clearer picture of the vibrational components involved. The absorption or emission spectra provide information of the strength of the resonance coupling of the control field, resulting in dynamical Stark splitting in the absorption and emission features. RAS spectroscopy can thus be a powerful alternative tool to transient absorption or emission spectroscopy in this nonlinear x-ray pump-probe setting. Moreover, Auger electron spectroscopy brings additional information on the final states of a system driven by a strong x-ray field, easily distinguishing single- and multi-ionized molecular states. This, together with the vibrational dynamics resolution, makes the RAS technique indispensable for strong-field XFEL applications. Our study also shows that XTAS cannot be simply understood or it is not easy to extract the dynamic information from XTAS of molecules, so further theoretical investigations of XTAS on the studies of molecules will be performed in the near future.

[1] K. Tiedtke, A. Azima, N. Von Bargen, L. Bittner, S. Bonfigt, S. Düsterer, B. Faatz, U. Frühling, M. Gensch, C. Gerth *et al.*, New J. Phys. **11**, 023029 (2009).

[2] E. Allaria, C. Callegari, D. Cocco, W. M. Fawley, M. Kiskinova, C. Masciovecchio, and F. Parmigiani, New J. Phys. **12**, 075002 (2010).

[3] C. Bostedt, S. Boutet, D. M. Fritz, Z. Huang, H. J. Lee, H. T. Lemke, A. Robert, W. F. Schlotter, J. J. Turner, and G. J. Williams, Rev. Mod. Phys. **88**, 015007 (2016).

[4] A. Marinelli, D. Ratner, A. A. Lutman, J. Turner, J. Welch, F.-J. Decker, H. Loos, C. Behrens, S. Gilevich, A. A. Miahnahri *et al.*, Nat. Commun. **6**, 6369 (2015).

[5] A. A. Lutman, R. Coffee, Y. Ding, Z. Huang, J. Krzywinski, T. Maxwell, M. Messerschmidt, and H.-D. Nuhn, Phys. Rev. Lett. **110**, 134801 (2013).

[6] J. Amann, W. Berg, V. Blank, F.-J. Decker, Y. Ding, P. Emma, Y. Feng, J. Frisch, D. Fritz, J. Hastings *et al.*, Nat. Photonics **6**, 693 (2012).

[7] D. Ratner, R. Abela, J. Amann, C. Behrens, D. Bohler, G. Bouchard, C. Bostedt, M. Boyes, K. Chow, D. Cocco *et al.*, Phys. Rev. Lett. **114**, 054801 (2015).

[8] W. Helml, A. R. Maier, W. Schweinberger, I. Grgura, P. Radcliffe, G. Doumy, C. Roedig, J. Gagnon, M. Messerschmidt, S. Schorb *et al.*, Nat. Photonics **8**, 950 (2014).

[9] N. Hartmann, W. Helml, A. Galler, M. R. Bionta, J. Grnert, S. L. Molodtsov, K. R. Ferguson, S. Schorb, M. L. Swiggers, S. Carron *et al.*, Nat. Photonics **8**, 706 (2014).

[10] K. Prince, E. Allaria, C. Callegari, R. Cucini, G. De Ninno, S. Di Mitri, B. Diviacco, E. Ferrari, P. Finetti, D. Gauthier *et al.*, Nat. Photonics **10**, 176 (2016).

[11] K. Schnorr, A. Senftleben, M. Kurka, A. Rudenko, L. Foucar, G. Schmid, A. Broska, T. Pfeifer, K. Meyer, D. Anielski *et al.*, Phys. Rev. Lett. **111**, 093402 (2013).

[12] K. Schnorr, A. Senftleben, M. Kurka, A. Rudenko, G. Schmid, T. Pfeifer, K. Meyer, M. Kübel, M. F. Kling, Y. Jiang *et al.*, Phys. Rev. Lett. **113**, 073001 (2014).

[13] B. Erk, R. Boll, S. Trippel, D. Anielski, L. Foucar, B. Rudek, S. W. Epp, R. Coffee, S. Carron, S. Schorb *et al.*, Science **345**, 288 (2014).

[14] B. McFarland, J. Farrell, S. Miyabe, F. Tarantelli, A. Aguilar, N. Berrah, C. Bostedt, J. Bozek, P. Bucksbaum, J. Castagna *et al.*, Nat. Commun. **5**, 4235 (2014).

[15] A. Petralia *et al.*, Phys. Rev. Lett. **115**, 014801 (2015).

[16] E. Allaria, F. Bencivenga, R. Borghes, F. Capotondi, D. Castronovo, P. Charalambous, P. Cinquegrana, M. Danailov, G. De Ninno, A. Demidovich *et al.*, Nat. Commun. **4**, 2476 (2013).

[17] T. Hara, Y. Inubushi, T. Katayama, T. Sato, H. Tanaka, T. Tanaka, T. Togashi, K. Togawa, K. Tono, M. Yabashi *et al.*, Nat. Commun. **4**, 2919 (2013).

[18] C. Pellegrini, A. Marinelli, and S. Reiche, Rev. Mod. Phys. **88**, 015006 (2016).

[19] A. Rudenko and D. Rolles, J. Electron Spectrosc. Relat. Phenom. **204**, 228 (2015).

[20] L. Fang, T. Osipov, B. Murphy, A. Rudenko, D. Rolles, V. Petrovic, C. Bostedt, J. Bozek, P. Bucksbaum, and N. Berrah, J. Phys. B: At., Mol. Opt. Phys. **47**, 124006 (2014).

[21] A. Picón, C. Lehmann, C. Bostedt, A. Rudenko, A. Marinelli, T. Osipov, D. Rolles, N. Berrah, C. Bomme, M. Bucher *et al.*, Nat. Commun. **7**, 11652 (2016).

[22] C. Lehmann, A. Picón, C. Bostedt, A. Rudenko, A. Marinelli, D. Moonshiram, T. Osipov, D. Rolles, N. Berrah, C. Bomme *et al.*, Phys. Rev. A **94**, 013426 (2016).

[23] I. Inoue, Y. Inubushi, T. Sato, K. Tono, T. Katayama, T. Kameshima, K. Ogawa, T. Togashi, S. Owada, Y. Amemiya *et al.*, Proc. Natl. Acad. Sci. USA **113**, 1492 (2016).

[24] N. Rohringer and R. Santra, Phys. Rev. A **77**, 053404 (2008).

[25] P. V. Demekhin, Y.-C. Chiang, and L. S. Cederbaum, Phys. Rev. A **84**, 033417 (2011).

[26] P. V. Demekhin and L. S. Cederbaum, J. Phys. B: At., Mol. Opt. Phys. **46**, 164008 (2013).

[27] A. D. Müller and P. V. Demekhin, J. Phys. B: At., Mol. Opt. Phys. **48**, 075602 (2015).

[28] A. Lindblad, V. Kimberg, J. Söderström, C. Nicolas, O. Travnikova, N. Kosugi, F. Gel'mukhanov, and C. Miron, New J. Phys. **14**, 113018 (2012).

[29] V. Kimberg, A. Lindblad, J. Söderström, O. Travnikova, C. Nicolas, Y. P. Sun, F. Gel'mukhanov, N. Kosugi, and C. Miron, Phys. Rev. X **3**, 011017 (2013).

[30] M. Piancastelli, M. Neeb, A. Kivimäki, B. Kempgens, H. Köppe, K. Maier, A. Bradshaw, and R. Fink, J. Phys. B: At., Mol. Opt. Phys. **30**, 5677 (1997).

[31] C. Ott, A. Kaldun, P. Raith, K. Meyer, M. Laux, J. Evers, C. H. Keitel, C. H. Greene, and T. Pfeifer, Science **340**, 716 (2013).

[32] C. Ott, A. Kaldun, L. Argenti, P. Raith, K. Meyer, M. Laux, Y. Zhang, A. Blättermann, S. Hagstotz, T. Ding *et al.*, Nature (London) **516**, 374 (2014).

[33] M. B. Gaarde, C. Buth, J. L. Tate, and K. J. Schafer, Phys. Rev. A **83**, 013419 (2011).

[34] W.-C. Chu and C. D. Lin, Phys. Rev. A **87**, 013415 (2013).

[35] X. Li, B. Birgitta, R. B. Annelise *et al.*, J. Phys. B: At., Mol. Opt. Phys. **48**, 125601 (2015).

[36] V. Kimberg and N. Rohringer, Phys. Rev. Lett. **110**, 043901 (2013).

[37] V. Kimberg, S. B. Zhang, and N. Rohringer, J. Phys. B: At., Mol. Opt. Phys. **46**, 164017 (2013).

[38] P. Skytt, P. Glans, K. Gunnelin, J. Guo, J. Nordgren, Y. Luo, and H. Agren, Phys. Rev. A **55**, 134 (1997).

[39] E. Pahl, H. D. Meyer, and L. S. Cederbaum, Z. Phys. D: At., Mol. Clusters **38**, 215 (1996).

[40] P. V. Demekhin and L. S. Cederbaum, Phys. Rev. A **83**, 023422 (2011).

[41] P. V. Demekhin and L. S. Cederbaum, Phys. Rev. A **86**, 063412 (2012).

[42] P. V. Demekhin and L. S. Cederbaum, Phys. Rev. Lett. **108**, 253001 (2012).

[43] S. B. Zhang and N. Rohringer, Phys. Rev. A **89**, 013407 (2014).

[44] E. Gamaly, *Femtosecond Laser-Matter Interaction: Theory, Experiments and Applications* (Pan Stanford Publishing Pte. Ltd., Singapore, 2011).

[45] B. W. Shore, *Manipulating Quantum Structures Using Laser Pulses* (Cambridge University Press, New York, 2011).

[46] L. S. Cederbaum and W. Domcke, J. Phys. B: At. Mol. Phys. **14**, 4665 (1981).

[47] W. Domcke, Phys. Rep. **208**, 97 (1991).

[48] G. A. Worth, M. H. Beck, A. Jackle *et al.*, The MCTDH Package, Version 8.2, (2000), University of Heidelberg, Heidelberg, Germany; H.-D. Meyer, Version 8.3 (2002), Version 8.4 (2007). See http://mctdh.uni-hd.de.

[49] H. Stapelfeldt and T. Seideman, Rev. Mod. Phys. **75**, 543 (2003).

[50] E. Kukk, J. D. Bozek, W. T. Cheng *et al.*, J. Chem. Phys. **111**, 9642 (1999).

[51] M. Neeb, J. Rubensson, M. Biermann, and W. Eberhardt, J. Electron Spectrosc. Relat. Phenom. **67**, 261 (1994).

[52] U. Fano, Phys. Rev. **124**, 1866 (1961).

[53] U. Fano and J. W. Cooper, Phys. Rev. **137**, A1364 (1965).

[54] S. Chatterjee and T. Nakajima, Phys. Rev. A **91**, 043413 (2015).

[55] C. D. Lin and W.-C. Chu, Science **340**, 694 (2013).

[56] K. Meyer, Z. Liu, N. Müller, J.-m. Mewes, A. Dreuw, T. Buckup, M. Motzkus, and T. Pfeifer, Proc. Natl. Acad. Sci. USA **112**, 201509201 (2015).

[57] A. K. Popov, V. V. Kimberg, and T. F. George, Phys. Rev. A **68**, 033407 (2003).

[58] A. K. Popov and V. V. Kimberg, Quantum Electron. **28**, 228 (1998).

[59] P. L. Knight, M. A. Lauder, and B. J. Dalton, Phys. Rep. **190**, 1 (1990).

[60] A. Zielinski, V. P. Majety, S. Nagele, R. Pazourek, J. Burgdorfer, and A. Scrinzi, Phys. Rev. Lett. **115**, 243001 (2015).